AMERICAN SOCIETY FOR MICROBIOLOGY | Journal of Virology®

VIRUS-CELL INTERACTIONS

Entry of Human Coronavirus NL63 into the Cell

Aleksandra Milewska,[a,b] Paulina Nowak,[a,b] Katarzyna Owczarek,[a,b] Artur Szczepanski,[a,b] Miroslaw Zarebski,[c] Agnieszka Hoang,[c] Krzysztof Berniak,[c] Jacek Wojarski,[d] Slawomir Zeglen,[d] Zbigniew Baster,[e] Zenon Rajfur,[e] Krzysztof Pyrc[a,b]

[a]Microbiology Department, Faculty of Biochemistry, Biophysics and Biotechnology, Jagiellonian University, Krakow, Poland

[b]Laboratory of Virology, Malopolska Centre of Biotechnology, Jagiellonian University, Krakow, Poland

[c]Department of Cell Biophysics, Faculty of Biochemistry, Biophysics and Biotechnology, Jagiellonian University, Krakow, Poland

[d]Department of Cardiac Surgery and Transplantology, Silesian Center for Heart Diseases, Zabrze, Poland

[e]Institute of Physics, Faculty of Physics, Astronomy and Applied Computer Sciences, Jagiellonian University, Krakow, Poland

ABSTRACT The first steps of human coronavirus NL63 (HCoV-NL63) infection were previously described. The virus binds to target cells by use of heparan sulfate proteoglycans and interacts with the ACE2 protein. Subsequent events, including virus internalization and trafficking, remain to be elucidated. In this study, we mapped the process of HCoV-NL63 entry into the LLC-Mk2 cell line and *ex vivo* three-dimensional (3D) tracheobronchial tissue. Using a variety of techniques, we have shown that HCoV-NL63 virions require endocytosis for successful entry into the LLC-MK2 cells, and interaction between the virus and the ACE2 molecule triggers recruitment of clathrin. Subsequent vesicle scission by dynamin results in virus internalization, and the newly formed vesicle passes the actin cortex, which requires active cytoskeleton rearrangement. Finally, acidification of the endosomal microenvironment is required for successful fusion and release of the viral genome into the cytoplasm. For 3D tracheobronchial tissue cultures, we also observed that the virus enters the cell by clathrin-mediated endocytosis, but we obtained results suggesting that this pathway may be bypassed.

IMPORTANCE Available data on coronavirus entry frequently originate from studies employing immortalized cell lines or undifferentiated cells. Here, using the most advanced 3D tissue culture system mimicking the epithelium of conductive airways, we systematically mapped HCoV-NL63 entry into susceptible cells. The data obtained allow for a better understanding of the infection process and may support development of novel treatment strategies.

KEYWORDS HCoV-NL63, clathrin, *Coronaviridae*, coronavirus, endocytosis, entry, infection, internalization

Human coronavirus NL63 (HCoV-NL63) was discovered shortly after the emergence of the severe acute respiratory syndrome coronavirus (SARS-CoV) (1). Extensive studies on the pathogen's biology and epidemiology revealed that it is prevalent worldwide, appearing with a seasonal distribution similar to that of other human coronaviruses. The clinical presentation may vary depending on the general health status of the patient. Usually, the virus causes a relatively mild respiratory tract disease, but fatal cases have been reported (2–5). Furthermore, broad studies on the association between infection and clinical symptoms reveal that HCoV-NL63 is associated with croup in young children (6–9).

Phylogenetically, HCoV-NL63 clusters within the genus *Alphacoronavirus*, which

Received 7 November 2017 **Accepted** 7 November 2017

Accepted manuscript posted online 15 November 2017

Citation Milewska A, Nowak P, Owczarek K, Szczepanski A, Zarebski M, Hoang A, Berniak K, Wojarski J, Zeglen S, Baster Z, Rajfur Z, Pyrc K. 2018. Entry of human coronavirus NL63 into the cell. J Virol 92:e01933-17. https://doi.org/10.1128/JVI.01933-17.

Editor Julie K. Pfeiffer, University of Texas Southwestern Medical Center

Address correspondence to Krzysztof Pyrc, k.a.pyrc@uj.edu.pl.

A.M. and P.N. contributed equally to this article.

also includes another human pathogen, HCoV-229E. Initially, these two viruses were considered distant relatives that diverged at some point due to an unknown reason. More recent research shows, however, that these two species most likely emerged in the human population during two separate zoonotic transmission events (10–12).

From the perspective of genome structure, HCoV-NL63 is similar to other alphacoronaviruses in that the 5′-terminal two-thirds of the genome encodes a large polyprotein, which is cleaved to yield several nonstructural proteins. Five genes (encoding S, ORF3, E, M, and N) are located at the 3′ terminus and encode structural proteins. The spike protein (S) is a class I fusion protein comprising a rod-like domain anchored to the virion via its C terminus and a globular head responsible for the interaction with cellular entry receptors (13). It is generally assumed that alphacoronaviruses interact with and enter host cells using CD13 (aminopeptidase N). However, HCoV-NL63 utilizes the ACE2 protein for this purpose, a characteristic shared only with SARS-CoV (14, 15). Virus tropism not only depends on the presence of a certain entry receptor but also may be modulated by other factors, e.g., attachment receptors, protease availability, and the activity of pathways responsible for internalization and trafficking of the virus particle (16, 17).

While binding to their cognate entry receptor provides sufficient stimulus for some viruses to initiate fusion between the viral and cellular membranes, most internalize via endocytosis; acidification and/or processing by cathepsins is then a prerequisite for fusion (13). For a long time, endocytic entry of virions was classified as clathrin dependent, clathrin independent, or clathrin and caveolin independent. During recent years, a number of other pathways were identified, and this complex machinery has become better understood. The occurrence, abundance, and mechanistic details of these pathways appear to vary between cell types, tissues, and species. Most often, the selection of a specific endocytic route is linked to cargo-directed trafficking and receptor-dependent trafficking. Nevertheless, many receptors/cargoes allow flexibility due to their capacity to enter a cell via multiple pathways.

The early stages of HCoV-NL63 infection have been described by us and others (18–20). Here, we made an effort to delineate events that occur early during HCoV-NL63 infection. First, the virus anchors to ciliated cells via heparan sulfate proteoglycans before interacting with the ACE2 entry receptor. Our results show that the virus-ACE2 interaction triggers recruitment of clathrin, followed by clathrin-mediated, dynamin-dependent endocytosis, which requires actin cortex remodeling. To ensure that our results were reliable, we used *ex vivo* cultured human airway epithelium (HAE), which mimics the microenvironment at the infection site.

RESULTS

HCoV-NL63 enters the cell via endocytosis. We first determined whether entry of HCoV-NL63 requires endocytosis and acidification of endosomes. For this, we studied the effect of ammonium chloride (NH_4Cl) and bafilomycin A, lysosomotropic agents that inhibit acidification of endosomes (21–23), using two models of HCoV-NL63 infection: permissive LLC-Mk2 cells and HAE cultures. Cells were preincubated with NH_4Cl (50 mM), bafilomycin A (100 nM), or control dimethyl sulfoxide (DMSO) for 1 h at 37°C and subsequently incubated with the virus at a 50% tissue culture infective dose ($TCID_{50}$) of 100/ml for LLC-Mk2 cells or 400/ml for HAE for 2 h at 32°C in the presence of the inhibitor. Subsequently, supernatants were removed, and cells were washed thrice with acidic buffer to inhibit the fusogenic activity of the virions retained on the surface (24). Next, LLC-Mk2 cells were washed with 1× phosphate-buffered saline (PBS) (pH 7.4), overlaid with culture medium, and incubated at 32°C for 4 days. Supernatant samples were collected for virus replication analysis. Simultaneously, HAE cultures were washed with 1× PBS (pH 7.4) and further maintained at an air-liquid interphase at 32°C for 5 days. During this time, HAE cultures were washed every 24 h with 1× PBS supplemented with a given inhibitor for 10 min at 32°C, and apical washes were collected for virus replication analysis. Subsequently, viral RNA was isolated and reverse

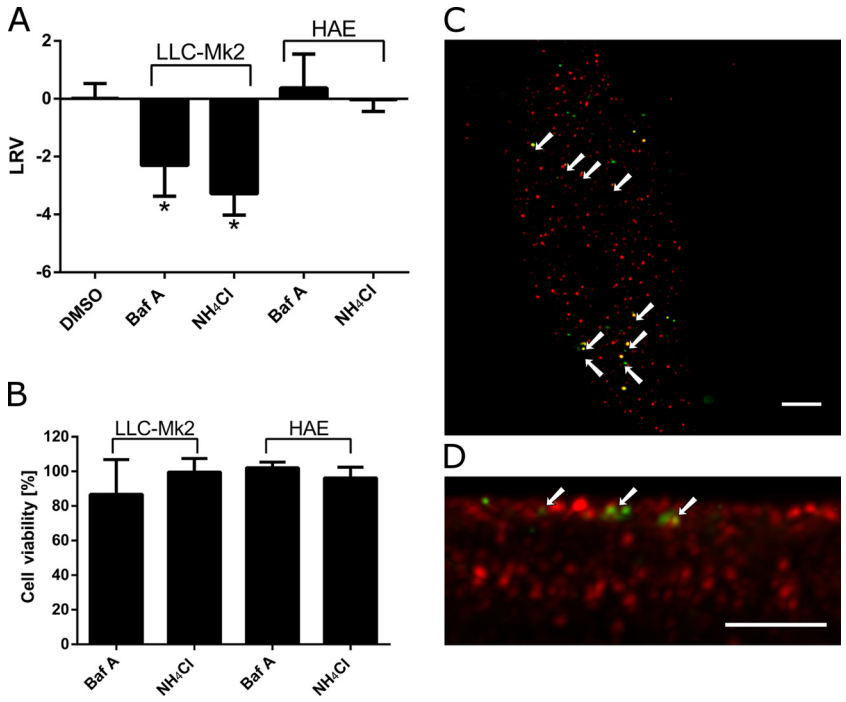

FIG 1 Importance of endosomal entry for HCoV-NL63 infection. (A) Inhibition of HCoV-NL63 infection in LLC-Mk2 cells and HAE cultures by the lysosomotropic agents ammonium chloride (NH_4Cl) (50 mM) and bafilomycin A (Baf A) (100 nM), as determined by RT-qPCR. Data on the *y* axis represent LRVs. The assay was performed in triplicate, and average values with standard errors are presented. *P* values of <0.05 were considered significant and are denoted with an asterisk. (B) The cytotoxicity of the tested inhibitors was measured with an XTT assay. Data on the *y* axis represent viability of the treated cells compared to the untreated reference samples. The assay was performed in triplicate, and average values with standard errors are presented. (C and D) Confocal images showing colocalization of HCoV-NL63 virions with the early endosomal marker EEA1 on LLC-Mk2 cells (C) and HAE cultures (D). Scale bars = 5 μm. Green, HCoV-NL63; red, EEA1.

transcribed (RT), and the HCoV-NL63 yield was determined using a quantitative real-time PCR (qPCR).

Bafilomycin A and NH_4Cl inhibited HCoV-NL63 infection in LLC-Mk2 cells, proving that acidification is a requirement for the virus infection *in vitro*. No inhibition was observed in HAE cultures (Fig. 1A). No cytotoxic effect was observed in the presence of these inhibitors (Fig. 1B).

Next, we analyzed HCoV-NL63 colocalization with early endosome antigen 1 (EEA1), a hydrophilic protein localizing exclusively to early endosomes (25). LLC-Mk2 cells were fixed after 10, 20, 30, or 40 min postinoculation (p.i.) with gradient-purified virus, stained with antibodies specific to HCoV-NL63 N protein and EEA1, and analyzed under a confocal microscope. Measured colocalization, expressed as Manders' coefficient, increases with time and reaches 0.68 at 40 min p.i. ($n = 6$ cells) (Fig. 1C).

We validated the obtained results using the HAE model. Briefly, HAE cultures were inoculated with gradient-purified HCoV-NL63 and incubated at 32°C for 2 h. For this culture model, a longer incubation was required to observe virus attachment and entry, most likely due to the requirement to cross the mucus layer. Subsequently, cells were fixed and labeled with specific antibodies against HCoV-NL63 N protein and EEA1. Colocalization of HCoV-NL63 virus particles with EEA1 protein was analyzed using a confocal microscope. Colocalization of virus and EEA1 was observed in inoculated cells (Fig. 1D).

Endocytosis of virus particles is induced by binding to the entry receptor. HCoV-NL63 virus employs the ACE2 protein for cellular entry, while heparan sulfate proteoglycans serve as attachment receptors (19). Here, we analyzed the consequence

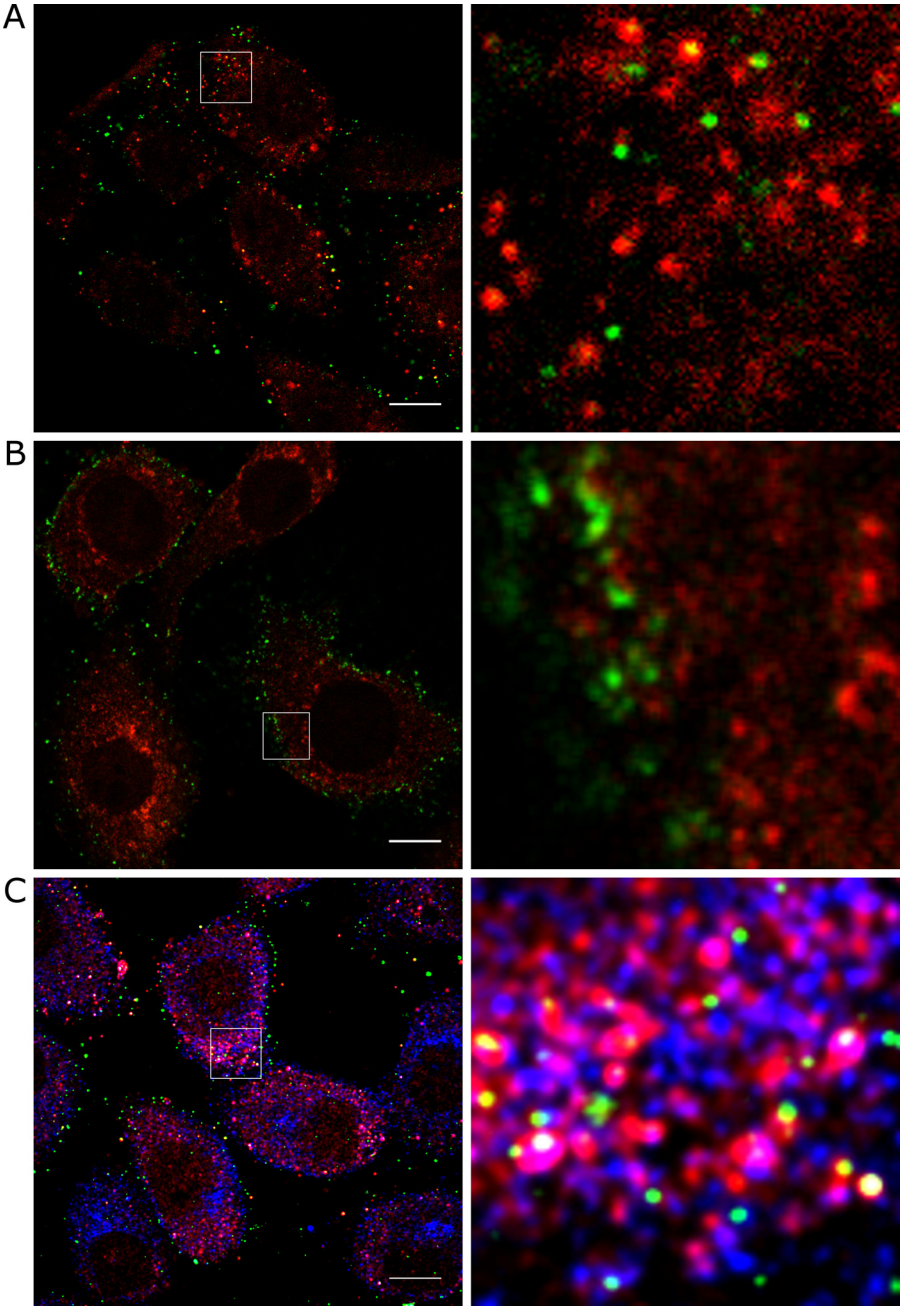

FIG 2 HCoV-NL63 binding to ACE2 triggers clathrin-mediated endocytosis. Precooled LLC-Mk2 cells were incubated with gradient-purified HCoV-NL63 for 40 min at 4°C following 0 min (A and B) or 5 min (C) of incubation at 32°C. Colocalization of the virus (green) and ACE2 (red) was analyzed using confocal microscopy (A). No colocalization with clathrin was observed after 0 min of incubation (B). Triple colocalization of virus with ACE2 and clathrin (blue) is visible in panel C. Images on the right side are zoomed-in regions indicated by white rectangles on the left-side slides. A representative image is shown. Scale bars = 10 μm.

of interaction between the virus particle and ACE2. First, we inoculated naturally permissive LLC-Mk2 cells with HCoV-NL63 and incubated them for 40 min at 4°C to enable virus adhesion to a cell surface. Subsequently cells were fixed, the virus was labeled with specific antibodies, and its colocalization with ACE2 and clathrin was studied. As shown in Fig. 2A, HCoV-NL63 particles attach efficiently to the cell surface. However, only a proportion of virions colocalize with the ACE2 (Manders' coefficient = 0.573; $n = 5$), suggesting that binding to the heparan sulfate precedes interaction with

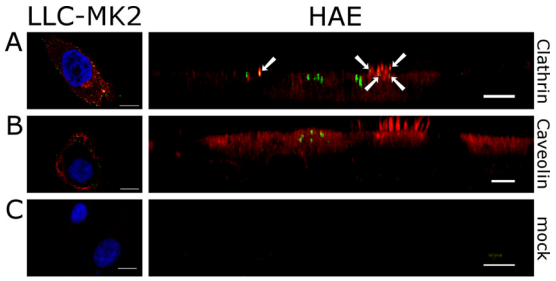

FIG 3 HCoV-NL63 colocalizes with clathrin but not caveolin. (A and B) LLC-Mk2 cells were incubated with gradient-purified HCoV-NL63 for 40 min at 4°C following 5 min (A) or 20 min (B) of incubation at 32°C. HAE cultures were incubated with gradient-purified HCoV-NL63 for 40 min at 4°C following 120 min of incubation at 32°C. HCoV-NL63 colocalization with clathrin (A) or caveolin (B) was analyzed with confocal microscopy (HCoV-NL63, green; clathrin and caveolin, red; nuclei, blue). (C) Cells mock incubated and stained with isotypic antibodies were used as a control. Scale bars = 5 μm.

the entry receptor. At that point, there is no colocalization of virus particles and clathrin-coated pits (Manders' coefficient = 0.140; $n = 5$) (Fig. 2B). Next, we tested whether the virus binding to the adhesion or entry receptor triggers recruitment of common cellular proteins responsible for pit formation by incubating cells for 5 min at 32°C. Immunostaining showed that the virus particles bound to ACE2 start to colocalize with clathrin (Manders' coefficient = 0.849; $n = 6$) (Fig. 2C), while there is no colocalization between non-ACE2-bound virions and clathrin (Manders' coefficient = 0.189; $n = 6$).

HCoV-NL63 colocalizes with clathrin during entry. To determine whether colocalization with clathrin following the ACE2 binding is relevant and the virus indeed enters the cell by use of clathrin-coated pits, we analyzed colocalization of intracellular virions with clathrin. Briefly, LLC-Mk2 cells were incubated at 32°C for 5 to 20 min with gradient-purified HCoV-NL63, fixed, immunostained, and analyzed by confocal microscopy. The results showed colocalization of virions entering the cell with clathrin (Manders' coefficient = 0.584; $n = 7$) (Fig. 3A), whereas no colocalization with caveolin 1 was observed (Manders' coefficient = 0.053; $n = 5$) (Fig. 3B). HCoV-NL63 colocalization with clathrin and caveolin was also studied in the HAE model. For this, cultures were incubated with gradient-purified HCoV-NL63 at 32°C for 2 h; the virus and the cellular proteins were immunostained and analyzed by confocal microscopy. HCoV-NL63 virions also colocalized with clathrin in this model, whereas no colocalization was observed for caveolin 1 (Fig. 3).

Clathrin and dynamin are important for HCoV-NL63 entry. As we already knew that HCoV-NL63 virions migrate to clathrin-coated pits, in the subsequent step we aimed to determine whether the clathrin-mediated endocytosis is indeed important for the virus entry. For this reason, we blocked the pathway using Pitstop 2 {*N*-[5-(4-bromobenzylidene)-4-oxo-4,5-dihydro-1,3-thiazol-2-yl]naphthalene-1-sulfonamide}, a selective clathrin inhibitor targeting its amino-terminal domain, and tetradecyltrimethylammonium bromide (MiTMAB), a dynamin I and II GTPase inhibitor. Activity of these compounds was verified with the positive control, fluorescently labeled transferrin (26, 27). LLC-Mk2 cells were treated with Pitstop 2, MiTMAB, or control DMSO for 30 min at 37°C following transferrin uptake for 45 min at 37°C. Confocal images showed that both inhibitors blocked transferrin endocytosis, as the protein was present only on the cell surface (Fig. 4A to D).

Subsequently, LLC-Mk2 cells were incubated with one of the inhibitors at 37°C for 30 min and inoculated with gradient-purified HCoV-NL63 at 32°C for 5 min. Following immunostaining of the HCoV-NL63 N protein and actin, virus endocytosis was analyzed using confocal microscopy. The results showed that virus internalization was hampered in cells pretreated with clathrin and dynamin inhibitors compared to the DMSO-treated cells (Fig. 4D to G). Simultaneously, a cytotoxicity test of the entry inhibitors was performed, which showed no toxic effect of the tested compounds on LLC-Mk2 cells

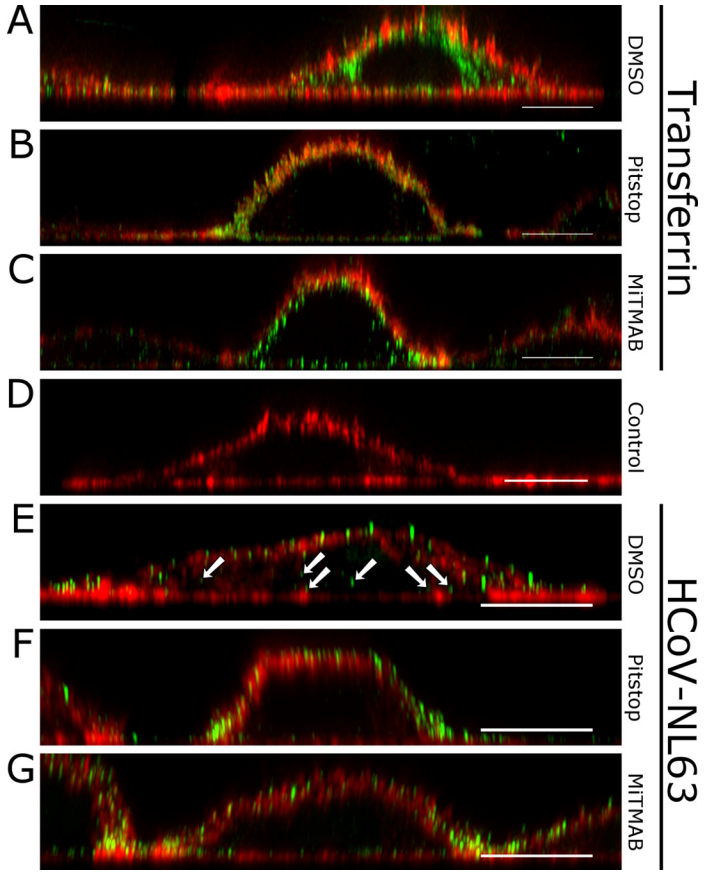

FIG 4 Clathrin and dynamin inhibitors hamper internalization of HCoV-NL63. (A to C) In order to verify the effectiveness of inhibitors, LLC-Mk2 cells were incubated with control DMSO (A), 10 μM Pitstop 2 (B), or 10 μM MiTMAB (C) for 30 min at 37°C and inoculated with Alexa Fluor 488-labeled transferrin. Following incubation (45 min, 37°C), cells were fixed and stained for actin (red). Transferrin entry was evaluated with confocal microscopy. (E to G) LLC-Mk2 cells were incubated with control DMSO (E), 10 μM Pitstop 2 (F), or 10 μM MiTMAB (G) for 30 min at 37°C. Cells were inoculated with purified HCoV-NL63 and incubated at 32°C for 1 h. Subsequently, cells were fixed and immunostained for HCoV-NL63 particles (green) and actin (red). (D) Mock-infected cells were used as a control. Scale bars = 10 μm.

(Fig. 5). In order to ensure that our observations were not biased, statistical analysis of virus entry was performed. For this, an algorithm was prepared for image analysis, a 3D representation of the cell was prepared, and the virus position in the cell was determined (Fig. 6).

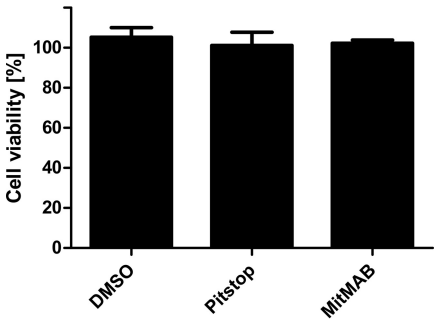

FIG 5 Cytotoxicity of Pitstop 2 and MiTMAB on LLC-Mk2 cells. The cytotoxicity of the endocytosis inhibitors was tested with an XTT assay. Cells were incubated with control DMSO, 10 μM Pitstop 2, or 10 μM MiTMAB for 2 h at 37°C Data on the *y* axis represent viability of the treated cells compared to the untreated reference samples. The assay was performed in triplicate, and average values with standard errors are presented.

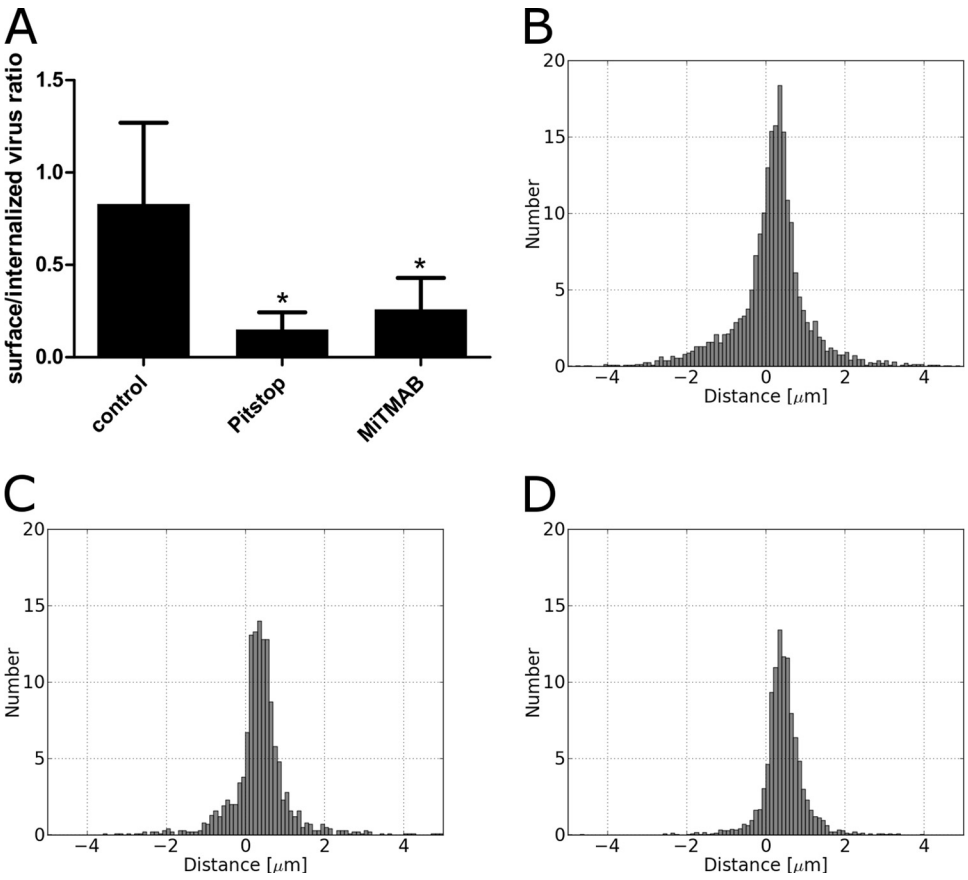

FIG 6 Numerical image analysis: clathrin and dynamin inhibitors block HCoV-NL63 entry. (B to D) LLC-Mk2 cells were incubated with DMSO (B), 10 μM MiTMAB (C), or 10 μM Pitstop 2 (D) for 30 min at 37°C and subsequently inoculated with purified HCoV-NL63 and incubated for 45 min at 32°C. Confocal images were digitalized, and the localization of each virus particle relative to the cellular membrane was assessed. (A) Number of internalized virus particles relative to number of virions on the cell surface (*y* axis) for cells treated with DMSO (control), Pitstop 2, or MiTMAB. In panels B, C, and D, raw data for cells treated with DMSO, Pitstop 2, or MiTMAB, respectively, are presented. Histograms show the average number of virus particles (*y* axis) versus the distance from the cell surface (*x* axis). Values of <0 on the *x* axis indicate that the virus is inside the cell, while for extracellular virions, the *x* value is ≥ 0.

A similar experiment was conducted using HAE cultures. For this, cultures were incubated for 1 h at 37°C with the inhibitors described above following incubation with gradient-purified HCoV-NL63 at 32°C for 2 h. A strong inhibition of virus internalization in cultures preincubated with clathrin or dynamin inhibitors compared to control cells was observed (Fig. 7). No cytotoxicity to HAE was observed for the tested inhibitors after 3 h of incubation at 37°C (Fig. 8).

Clathrin-mediated endocytosis is the main entry route for HCoV-NL63. Even though certain cargo is usually internalized by a single route, frequently other pathways may be used as alternatives. We therefore aimed to test whether inhibition of clathrin-mediated entry with chemical inhibitors results in inhibition of virus replication. To address this, we incubated LLC-Mk2 cells with a given inhibitor at 37°C for 1 h and infected them with HCoV-NL63 ($TCID_{50}$ = 400 per ml) for 2 h at 32°C. Subsequently, media were removed and cells were washed thrice with acidic buffer following washing with 1× PBS (pH 7.4). Next, cells were overlaid with culture medium containing a given inhibitor and incubated at 32°C for 4 days. Cells were fixed and immunostained for HCoV-NL63 N protein to assess the number of infected cells. To assess the nonspecific effect of entry inhibitors, control cells were also treated with these at 4 h p.i. Clearly, in the presence of clathrin-mediated endocytosis inhibitors (Pitstop 2 and MiTMAB), the number of HCoV-NL63-infected cells was much lower than in the control. However, MiTMAB also inhibited virus replication at later stages of the infection (Fig. 9). To ensure

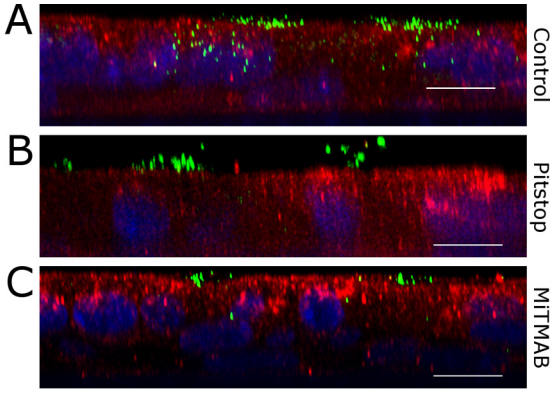

FIG 7 Clathrin and dynamin inhibitors prevent HCoV-NL63 from entering the cell in the HAE model. HAE cultures were incubated with control DMSO (A), 10 μM Pitstop 2 (B), or 10 μM MiTMAB (C) for 1 h at 37°C. Cells were then inoculated with purified HCoV-NL63 and incubated at 32°C for 2 h. Subsequently, cells were fixed and immunostained for HCoV-NL63 particles (green), actin (red), and nuclei (blue). Scale bars = 5 μm.

that entry inhibitors affected HCoV-NL63 infection in LLC-Mk2 cells, we analyzed by RT-qPCR virus replication at 120 h p.i. in the presence of the tested compounds. The analysis showed an ~2-log decrease in virus progeny production in the presence of Pitstop 2 and MiTMAB compared to that in DMSO-treated cells and a slight increase of RNA copy levels in the presence of nystatin (Fig. 10A). Importantly, no cytotoxic effect was observed for the tested inhibitors applied to LLC-Mk2 cells for 4 days at 32°C (Fig. 10B). The influence of the tested inhibitors on HCoV-NL63 infection was also analyzed in HAE cultures. For this, cultures were preincubated with a given inhibitor (Pitstop 2, MiTMAB, nystatin, or control DMSO) for 1 h at 37°C and infected with HCoV-NL63 at a $TCID_{50}$ of 400 per ml for 2 h at 32°C. Subsequently, noninternalized virions were inactivated by acid washing, and cultures were washed with 1× PBS and incubated with a given inhibitor for 10 min. After that time, supernatants were discarded and cultures were incubated for 5 days at 32°C. During this period, cultures were incubated with a given inhibitor for 10 min at 32°C every 24 h. Viral RNA from these samples was quantified by RT-qPCR. Virus replication in HAE was not affected by any of the tested inhibitors (Fig. 10A).

TMPRSS2 is important during early stages of the infection. It was previously suggested that coronaviruses may bypass the endocytic entry route employing transmembrane protease serine 2 (TMPRSS2), which primes the fusion protein and enables fusion of viral and cellular membranes on the cell surface (28, 29). We have tested

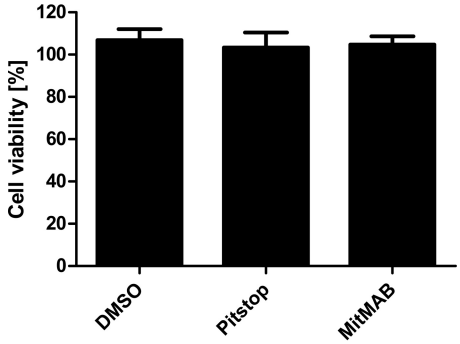

FIG 8 Cytotoxicity of Pitstop 2 and MiTMAB on HAE cultures. The cytotoxicity of the endocytosis inhibitors was tested with an XTT assay. Cells were incubated with control DMSO, 10 μM Pitstop 2, or 10 μM MiTMAB for 2 h at 37°C. Data on the *y* axis represent the viability of the treated cells compared to the untreated reference samples. The assay was performed in triplicate, and average values with standard errors are presented.

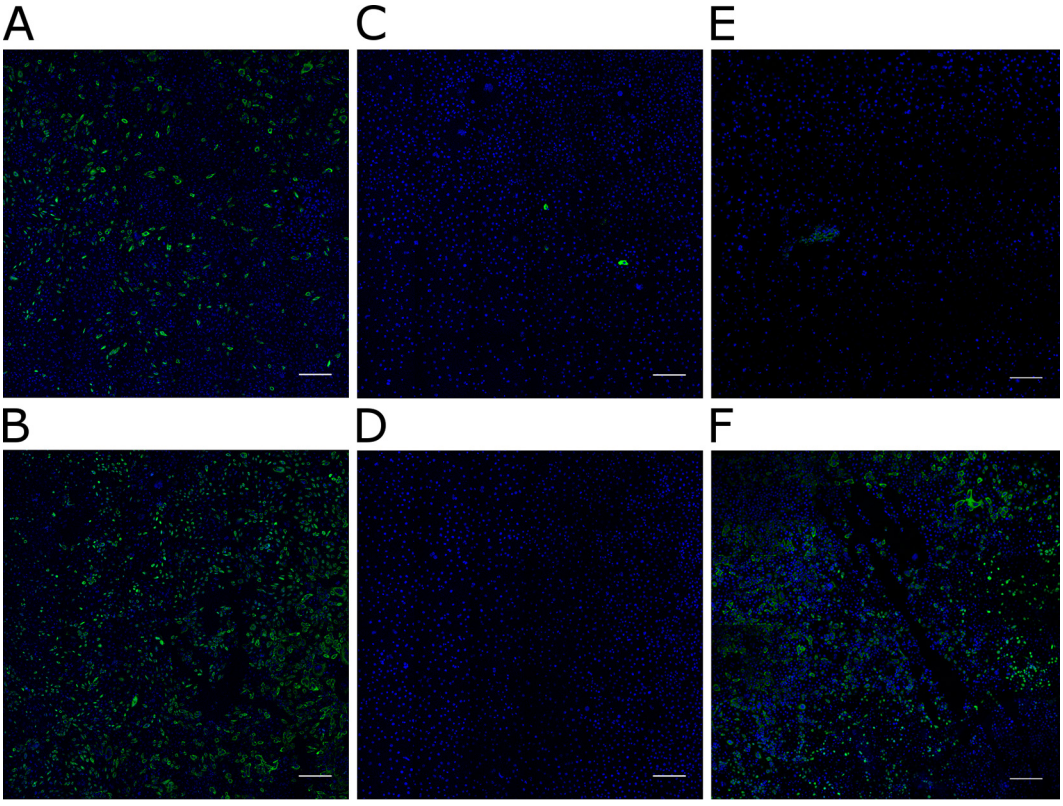

FIG 9 Clathrin and dynamin inhibitors limit the number of LLC-Mk2 infected cells. (A to D) LLC-Mk2 cells were incubated with control DMSO (A), 5 μg/ml nystatin (B), 10 μM MiTMAB (C), or 10 μM Pitstop 2 (D) for 1 h at 37°C and inoculated with HCoV-NL63 ($TCID_{50}$ = 100/ml). After 2 h of incubation at 32°C, virions that were not internalized were inactivated with acidic buffer (pH 3), and cells were incubated for 4 days at 32°C in the presence of the tested inhibitors or control DMSO. (E and F) The identical procedure was applied to cells, but in these MiTMAB (E) and Pitstop 2 (F) were applied after the acid wash. Fixed cells were immunostained with anti-NL63 nucleocapsid protein (green) and nuclei (blue), and confocal images were collected. Scale bar = 200 μm.

whether inhibition of TMPRSS2 with camostat affects the HCoV-NL63 infection. We observed that inhibition of TMPRSS2 hampers virus infection in HAE cultures, while it has no effect on virus replication in LLC-MK2 cells (Fig. 11A). No inhibition of virus entry was observed in any of the models, as tracked with confocal microscopy visualizing the nucleoprotein (Fig. 11B). As only single entry events per view were observed, several images for camostat-treated and control cells are presented. In total, 500 entry events into HAE cells were tracked, and no difference between the camostat-treated sample and the control sample was noted.

HCoV-NL63 entry requires actin remodeling. We studied trafficking of HCoV-NL63 inside the cell. As entry by endocytosis would probably require remodeling of the cytoskeleton, we evaluated virus internalization in the presence of cytochalasin D, jasplakinolide, or nocodazole. The first chemical inhibits actin polymerization, whereas the second binds F-actin and stabilizes actin filaments (30, 31). The last compound interferes with microtubule formation. The analysis showed that actin inhibitors prevented virus particles from penetrating the cell, with visible viral particle accumulation on actin cortex or unstructured actin deposits. The microtubule inhibitor did not affect virus entry (Fig. 12). No cytotoxicity was observed for the tested inhibitors (Fig. 13).

DISCUSSION

Previously, we and others described the first steps of the HCoV-NL63 infection process, showing that it begins with the virus binding to the cellular membrane via heparan sulfate proteoglycans, which then enable/facilitate interaction with the entry receptor, ACE2 (14, 18, 19). Little is known about the subsequent virus internalization

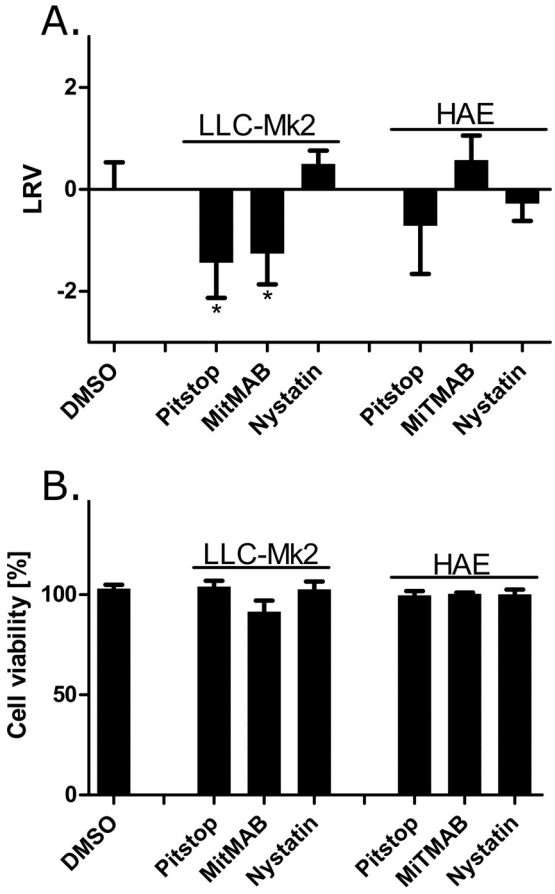

FIG 10 Clathrin and dynamin inhibitors hamper replication of HCoV-NL63 in LLC-MK2 cells. (A) HCoV-NL63 replication in LLC-Mk2 cells and HAE cultures in the presence of entry inhibitors or control DMSO was analyzed using RT-qPCR. Cultures were incubated with 10 μM Pitstop 2, 10 μM MiTMAB, 5 μg/ml nystatin, or DMSO for 1 h at 37°C and inoculated with HCoV-NL63 ($TCID_{50}$ = 400/ml). After 2 h of incubation at 32°C, virions that were not internalized were inactivated with acidic buffer (pH 3), and cells were incubated for 5 days at 32°C. The data are presented as log reduction value (LRV) compared to the control sample. The assay was performed in triplicate, and average values with standard errors are presented. *P* values of <0.05 were considered significant and are denoted with an asterisk. (B) The cytotoxicity of the inhibitors was tested with an XTT assay. Cells were incubated with 10 μM Pitstop 2, 10 μM MiTMAB, 5 μg/ml nystatin, or DMSO for 5 days at 32°C. Data on the *y* axis represent viability of the treated cells compared to the untreated reference samples. The assay was performed in triplicate, and average values with standard errors are presented.

and its trafficking through the cytoplasm, and some published data are contradictory. For example, the role played by cathepsins and acidification of the microenvironment during transition of the HCoV-NL63 S protein to its fusogenic form remains unclear.

We made an effort to systematically examine every step of the process. First, we tested whether the virus requires endocytosis for successful entry. To do this, we carried out experiments using chemical inhibitors of endosome acidification (ammonium chloride and bafilomycin A). Both blocked virus infection in LLC-MK2 cells, suggesting a requirement for transport of virions to endosomes, which then undergo acidification. However, such an approach may have several disadvantages. First, we examined the role of endosome acidification based on virus replication; thus, we cannot rule out interference with virus infection at later stages (as shown for MiTMAB). Second, the specificity and selectivity of chemical inhibitors are questionable. An indirect proof of the pH dependence of HCoV-NL63 entry may be provided by the fact that acidification of the environment (acid wash) results in inactivation of the virus, suggesting a pH-directed structural switch in the S protein. To further confirm our observations, we

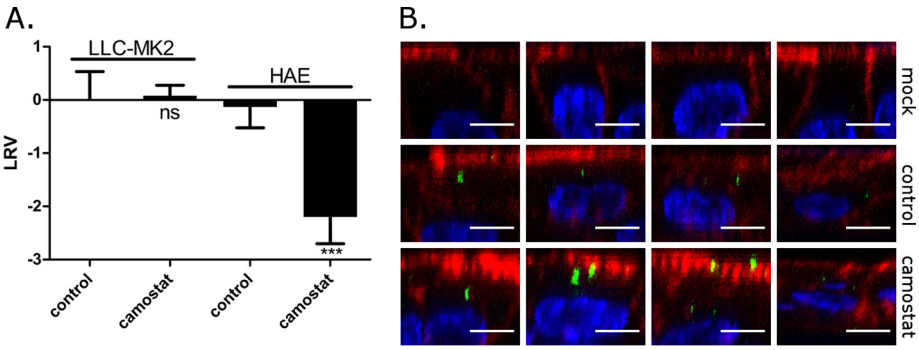

FIG 11 TMPRSS2 is required for entry into HAE cells but does not enable virus-cell fusion on the cell surface. (A) HCoV-NL63 replication in LLC-Mk2 cells and HAE cultures in the presence of camostat or control DMSO was analyzed using RT-qPCR. Cultures were incubated with 100 μM camostat or DMSO for 1 h at 37°C and inoculated with HCoV-NL63 ($TCID_{50}$ = 400/ml). After 2 h of incubation at 32°C, virions that were not internalized were inactivated with acidic buffer (pH 3), and cells were incubated for 5 days at 32°C. The data are presented as log reduction value (LRV) compared to the control sample. The assay was performed in triplicate, and average values with standard errors are presented. *P* values of <0.05 were considered significant and are denoted with asterisks. (B) HAE cultures were incubated with control DMSO or 100 μM camostat for 1 h at 37°C. Further, cells were inoculated with purified HCoV-NL63 and incubated at 32°C for 2 h. Subsequently, cells were fixed and immunostained for HCoV-NL63 particles (green), actin (red), and nuclei (blue). Scale bars = 5 μm.

developed a method of visualizing single virions as they entered the cell. Efforts to stain for virus surface proteins yielded poor results, most likely due to the lack of highly specific antibodies and posttranslational modification of surface proteins, and the best results were obtained when antibodies specific to the N protein were used. Incubation of cells with purified virions resulted in virus attachment, which was visualized by confocal microscopy and costaining for markers of the most commonly employed endocytic pathways and allowed us to study the colocalization. If significant colocalization was detected, the results were confirmed with chemical inhibitors.

The results showed that HCoV-NL63 binding to ACE2 initiates recruitment of clathrin and subsequent formation of clathrin-coated pits; no colocalization of the virus with other markers (e.g., caveolin) was noted. Transferrin was used as a positive control for clathrin-mediated endocytosis (32, 33). Importantly, chemical inhibitors of clathrin completely blocked virus internalization, and the virus remained on the cell surface. Analysis of HAE cultures yielded identical results. The inhibitors of endocytosis also hampered virus infection on LLC-Mk2 cells, highlighting that this pathway is relevant and the lack of an equally effective alternative entry route in this culture model. Clathrin-mediated endocytosis requires a number of other proteins, such as dynamin, the GTPase responsible for scission of clathrin-coated vesicles from the cell surface (34). Inhibiting dynamin also hampered virus internalization into LLC-MK2 cells and HAE cultures, confirming our previous observations. However, in this case the MiTMAB compound blocked replication of HCoV-NL63 also during subsequent stages of the infection.

It is noteworthy that we were not able to block virus infection of HAE cultures using inhibitors of endocytosis. This may be related to the fact that the cultures were exposed to inhibitors for a very short time during apical washes, which is not sufficient to permanently block the infection. On the other hand, it is also possible that in HAE, HCoV-NL63 is able to enter the cell by an alternative route. Recent reports on other coronaviruses (28, 29, 35) suggested that these viruses may bypass the endocytic entry route using TMPRRS2 as the priming protease, enabling entry directly from the cell surface. Our experiments showed that inhibition of this protease indeed inhibited virus infection. Interestingly, it did not hamper virus internalization into the cell. Our data are consistent with the data presented by others (28, 29, 35), yet we believe that there is a different mechanistic explanation for the observed phenomenon. We believe that

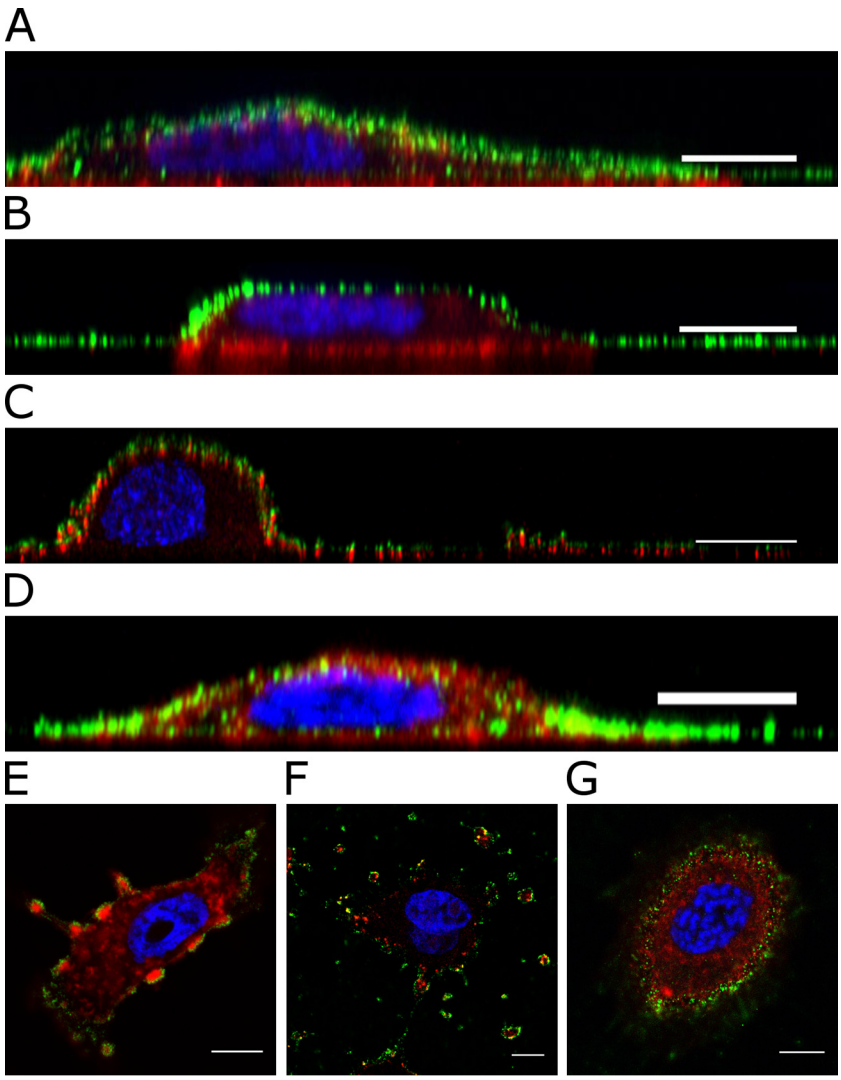

FIG 12 Actin is important for HCoV-NL63 entry. LLC-MK2 cells were incubated with DMSO (A), 10 μM cytochalasin D (B and E), 1.5 μM jasplakinolide (C and F), or 400 nM nocodazole (D and G) for 1 h at 37°C and then inoculated with purified HCoV-NL63 and incubated at 32°C for 1 h. Actin and virus localization was verified with confocal microscopy; fixed cells were immunostained for HCoV-NL63 particles (green), actin (red), and nuclei (blue). Scale bars = 10 μm.

TMPRRS2 indeed is required for the virus-cell fusion, acting similarly to cathepsins, but it does not enable fusion on the cell surface, and the acidification of the microenvironment is required.

Our final research question was about virus trafficking. The endosome typically translocates through the depolymerizing actin cortex and is subsequently sorted at the endosomal hub and directed to different destinations. This sorting is highly dependent on the cargo. Using two chemical inhibitors (jasplakinolide and cytochalasin B) (31, 36), we showed that actin plays a vital role in virus entry. Stabilization of the actin cortex using jasplakinolide resulted in immobilization of the virus at the cell surface, similarly to the case for inhibition of actin polymerization using cytochalasin D. These two experiments suggest a scenario in which virus-carrying endosomes pass along the actin cortex, which actively unwinds and interacts with virions.

In summary, we show that HCoV-NL63 enters the cell by clathrin-mediated endocytosis, but the pathway may be bypassed to some extent during infection *ex vivo*. HCoV-NL63 entry into the susceptible cell is summarized in Fig. 14.

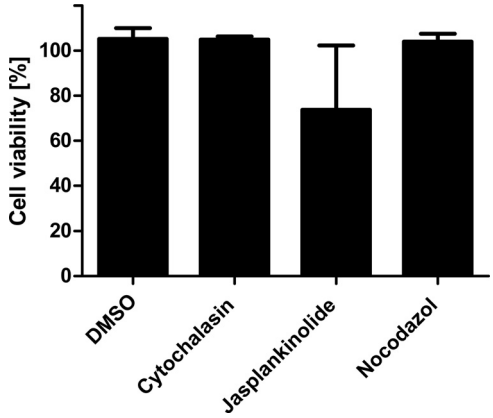

FIG 13 Cytotoxicity of the cytoskeleton-modifying compounds. The cytotoxicity of the endocytosis inhibitors was tested with an XTT assay. Cells were incubated with DMSO, 10 μM cytochalasin D, 1.5 μM jasplakinolide, or 400 nM nocodazole for 2 h at 37°C. Data on the *y* axis represent viability of the treated cells compared to the untreated reference samples. The assay was performed in triplicate, and average values with standard errors are presented.

MATERIALS AND METHODS

Cell culture. LLC-Mk2 cells (ATCC CCL-7; *Macaca mulatta* kidney epithelial) were maintained in minimal essential medium (MEM) (two parts Hanks' MEM and one part Earle's MEM; Thermo Fisher Scientific, Poland) supplemented with 3% heat-inactivated fetal bovine serum (Thermo Fisher Scientific, Poland), penicillin (100 U/ml), streptomycin (100 μg/ml), and ciprofloxacin (5 μg/ml). Cells were cultured at 37°C under 5% CO_2.

Ethics statement. Human tracheobronchial epithelial cells were obtained from airway specimens resected from adult patients undergoing surgery under Silesian Center for Heart Diseases-approved protocols. This study was approved by the Bioethical Committee of the Medical University of Silesia in Katowice, Poland (approval no. KNW/0022/KB1/17/10 dated 16 February 2010). Participants provided their written informed consent to participate in the study, as approved by the Bioethical Committee.

HAE cultures. Primary human tracheobronchial epithelial cells were expanded on plastic to generate passage 1 cells and plated on permeable Transwell insert (6.5-mm-diameter) supports. Human airway epithelium (HAE) cultures were generated by provision of an air-liquid interface for 6 to 8 weeks to form well-differentiated, polarized cultures that resemble *in vivo* pseudostratified mucociliary epithelium. Cultures were prepared and maintained as previously described (24).

Cell viability assay. LLC-Mk2 cells were cultured on 96-well plates, and HAE cultures were prepared as described above. Cell viability assay was performed by using the 2,3-bis-(2-methoxy-4-nitro-5-sulfophenyl)-2H-tetrazolium-5-carboxanilide salt (XTT) cell viability assay (Biological Industries, Israel) according to the manufacturer's instructions. Briefly, on the day of the assay, 100 μl of the culture medium (for LLC-Mk2) or 1× PBS (for HAE) with 30 μl of the activated XTT solution was added to each well/culture insert. Following 2 h of incubation at 37°C, the solution was transferred onto a 96-well plate

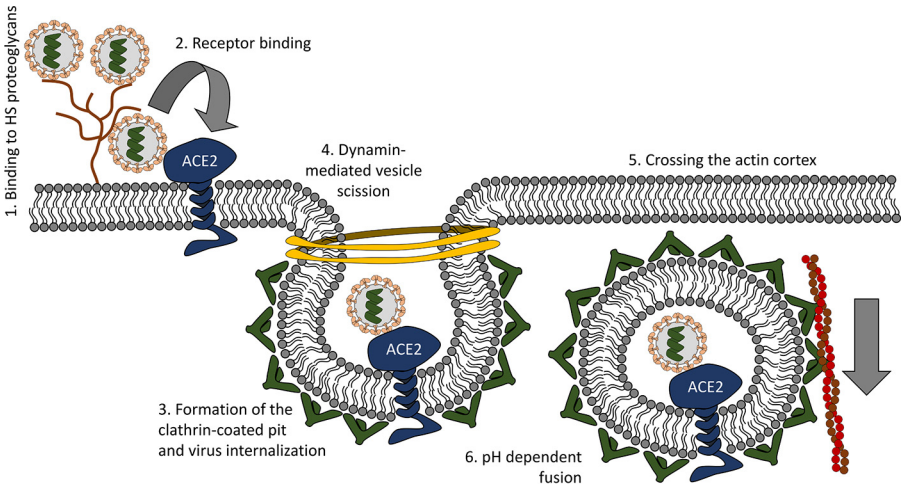

FIG 14 Early events during HCoV-NL63 infection.

and the signal was measured at $\lambda = 490$ nm using a colorimeter (Spectra Max 250; Molecular Devices). The results obtained were further normalized to the control sample, for which cell viability was set to 100%.

Virus preparation and titration. The HCoV-NL63 stock (isolate Amsterdam 1) was generated by infecting monolayers of LLC-Mk2 cells. The virus-containing liquid was aliquoted and stored at −80°C. A control LLC-Mk2 cell lysate from mock-infected cells was prepared in the same manner. The virus yield was assessed by titration on fully confluent LLC-Mk2 cells in 96-well plates according to the method described by Reed and Muench (37).

Purification of HCoV-NL63. The virus stock was concentrated 25-fold using centrifugal protein concentrators (Amicon Ultra, 10-kDa cutoff; Merck, Poland) and subsequently overlaid on 15% iodixanol solution in 1× PBS (OptiPrep medium; Sigma-Aldrich, Poland). Following virus concentration using an iodixanol cushion (centrifugation at 175,000 × *g* for 3 h at 4°C), it was overlaid on a 10 to 20% iodixanol gradient in 1× PBS and centrifuged at 175,000 × *g* for 18 h at 4°C. Fractions (1 ml) collected from the gradient were analyzed by Western blotting using anti-HCoV-NL63 N IgGs (0.25 μg/ml; Ingenansa, Spain) and a secondary antibody coupled with horseradish peroxidase (65 ng/ml; Dako, Denmark). The virus-containing fractions were aliquoted and stored at −80°C. The control cell lysate (mock) was concentrated and prepared in the same manner as the virus stock.

Inhibition of virus entry. LLC-Mk2 cells were seeded on coverslips in six-well plates (TPP, Switzerland) and cultured for 2 days at 37°C. Subsequently, cells were incubated with a given inhibitor for 30 min at 37°C and later with 50 μl of purified HCoV-NL63 or mock sample for 1 h at 32°C. For the *ex vivo* experiment, HAE cultures were exposed to the tested inhibitor or control PBS for 1 h at 37°C following inoculation with iodixanol-concentrated HCoV-NL63 or mock sample. Following 2 h of incubation at 32°C, unbound virions were removed by washing with 1× PBS. Cells were then washed with 1× PBS and fixed with 4% paraformaldehyde (PFA).

Transferrin and albumin were used as positive controls, as they were previously described to serve as a cargo in clathrin- and caveolin-dependent endocytosis, respectively (38, 39). LLC-Mk2 cells were seeded on coverslips in six-well plates (TPP, Switzerland) and cultured for 2 days at 37°C. Subsequently, cells were incubated with a given inhibitor for 30 min at 37°C following incubation with Alexa Fluor 488-labeled transferrin (100 μg/ml; Molecular Probes), fluorescein isothiocyanate (FITC)-labeled albumin (500 μg/ml; Sigma-Aldrich, Poland), or control PBS for 45 min at 32°C. Cells were then washed with 1× PBS and fixed in 4% PFA.

Immunostaining and confocal imaging. Fixed cells were permeabilized with 0.1% Triton X-100 in 1× PBS and incubated overnight at 4°C in 1× PBS supplemented with 5% bovine serum albumin (BSA) and 0.5% Tween 20. To visualize HCoV-NL63 particles, cells were incubated for 2 h at room temperature with mouse anti-HCoV-NL63 N IgGs (0.25 μg/ml; Ingenansa, Spain), followed by 1 h of incubation with Alexa Fluor 488-labeled goat anti-mouse IgG (2.5 μg/ml; Thermo Fisher Scientific, Poland). The following antibodies were used for endosomal markers: polyclonal goat anti-human clathrin HC coupled with tetramethylrhodamine (10 μg/ml; Santa Cruz Biotechnology), polyclonal rabbit anti-human early endosome antigen 1 (2 μg/ml; Santa Cruz Biotechnology), polyclonal rabbit anti-human caveolin 1 (2 μg/ml; Sigma-Aldrich, Poland), and Alexa Fluor 633-labeled goat anti-rabbit (2.5 μg/ml; Thermo Fisher Scientific, Poland). Actin filaments was stained using phalloidin coupled with Alexa Fluor 633 (0.2 U/ml; Thermo Fisher Scientific, Poland). Nuclear DNA was stained with DAPI (4′,6′-diamidino-2-phenylindole) (0.1 μg/ml; Sigma-Aldrich, Poland). Immunostained cultures were mounted on glass slides in ProLong Gold antifade medium (Thermo Fisher Scientific, Poland). Fluorescent images were acquired under a Leica TCS SP5 II confocal microscope (Leica Microsystems GmbH, Mannheim, Germany) and a Zeiss LSM 710 confocal microscope (Carl Zeiss Microscopy GmbH). Images were acquired using Leica Application Suite Advanced Fluorescence LAS AF v. 2.2.1 (Leica Microsystems CMS GmbH) or ZEN 2012 SP1 software (Carl Zeiss Microscopy GmbH) deconvolved with Huygens Essential package version 4.4 (Scientific Volume Imaging B.V., The Netherlands) and processed using ImageJ 1.47v (National Institutes of Health, Bethesda, MD, USA).

Flow cytometry. LLC-Mk2 cells were seeded on 6-well plates (TPP) and cultured for 2 days at 37°C with 5% CO_2. Cells in monolayer were incubated with each entry inhibitor for 1 h at 37°C following infection with HCoV-NL63 at a $TCID_{50}$ of 100/ml or inoculation of the mock sample. On day 4 p.i., cells were washed with sterile PBS, fixed with 3% PFA, permeabilized with 0.1% Triton X-100 in 1× PBS, and incubated for 1 h with 3% BSA in 1× PBS with 0.1% Tween 20. To quantify HCoV-NL63 infection, fixed cells were scraped from the plastic and incubated for 2 h at room temperature with mouse anti-HCoV-NL63 N IgG antibodies (1 μg/ml; Ingenansa), followed by 1 h of incubation with Alexa Fluor 488-labeled goat anti-mouse antibody (2.5 μg/ml; Molecular Probes). Cells were then washed, resuspended in 1× PBS, and analyzed with a FACSCalibur instrument (Becton Dickinson) using Cell Quest software.

Isolation of nucleic acids and reverse transcription. Viral nucleic acids were isolated from cell culture supernatants (LLC-Mk2 cells) or apical washes (HAE cultures) using the viral RNA/DNA isolation kit (A&A Biotechnology, Poland) according to the manufacturer's instructions. Reverse transcription was carried out with a high-capacity cDNA reverse transcription kit (Thermo Fisher Scientific, Poland), according to the manufacturer's instructions.

RT-qPCR. The HCoV-NL63 yield was determined by RT-qPCR (7500 Fast Real-Time PCR machine; Life Technologies, Poland). Viral cDNA (2.5 μl per sample) was amplified in a 10-μl reaction mixture containing 1× master mix (RT Mix Probe; A&A Biotechnology, Poland), a specific probe labeled with 6-carboxyfluorescein (FAM) and 6-carboxytetramethylrhodamine (TAMRA) (100 nM) (5′-ATG TTA TTC AGT GCT TTG GTC CTC GTG AT-3′), and primers (450 nM each) (sense, 5′-CTG TGG AAA ACC TTT GGC ATC-3′; antisense, 5′-CTG TGG AAA ACC TTT GGC ATC-3′). Rox was used as the reference dye. The reaction

conditions were as follows: 2 min at 50°C and 10 min at 92°C, followed by 40 cycles of 15 s at 92°C and 1 min at 60°C. In order to assess the copy number for the N gene, DNA standards were prepared. Briefly, the N gene of HCoV-NL63 was amplified and cloned into pTZ57R/T (Thermo Fisher Scientific, Poland) plasmid using the InsTAclone PCR cloning kit (Thermo Fisher Scientific, Poland). Subsequently, DNA vectors were amplified and linearized with EcoRI restriction enzyme. Linear nucleic acids were further purified with the GeneJET PCR purification kit (Thermo Fisher Scientific, Poland) according to the manufacturer's instructions, and its concentration was assessed using a spectrophotometer. The number of DNA copies per milliliter was assessed using Avogadro's constant and the molecular mass of RNA molecules. Samples were serially diluted and used as an input for real-time PCR.

In this article, the data from quantitative PCR are presented as log removal values (LRVs) in order to enable comparison of results obtained from different assays. The LRV was calculated according to the formula LRV $= -\log (c_i/c_0)$, where c_i is the number of viral RNA copies per milliliter in the sample from the culture treated with a given polymer and c_0 is the number of viral RNA copies per milliliter in the control sample (untreated cells).

Image analysis. To evaluate the infection inhibition in the presence of various endocytosis inhibitors, image analysis was performed on 2-mm by 2-mm tile scan images. On each image, the number of nuclei (expressed as a number of cells) and the mean pixel intensity for the virus were calculated. For that, histograms of all images were adjusted to the minimum/maximum value, excluding signal from the virus derived from images with no infected cells. Results are presented as mean intensity of fluorescence per cell.

Colocalization analyses were performed under ImageJ using the JACoP plugin (41), where Manders' coefficient was calculated for 3D images of more than 5 cells.

Quantitative analysis of virus internalization in the presence of inhibitors was performed with the algorithm previously described by Berniak et al. with modifications (40). The cell surface was estimated on each image slice manually using the polygon selection tool in ImageJ, and based on this information, the 3D cell surface was modeled. Coordinates of virus particles were determined using the 3D Object Counter ImageJ plugin. The relative localization and distance between the virus particle and cell surface were calculated. Results are presented as a ratio between virus particles inside a cell and the particles on the surface (up to 1.5 μm above).

Statistical analysis. All the experiments were performed in triplicate, and the results are presented as mean $\pm$ standard deviation (SD). To determine the significance of the obtained results, a comparison between groups was conducted using the Student *t* test. *P* values of <0.05 were considered significant.

ACKNOWLEDGMENTS

This work was supported by grants from the National Science Center (UMO-2012/07/E/NZ6/01712, UMO-2012/07/N/NZ6/02955, and 2015/19/N/NZ1/00323 to K.P., A.M., and K.B., respectively) and the Ministry of Science and Higher Education (0058/DIA/2015/44 to P.N.). K.P. acknowledges a networking contribution from the COST Action CM1407 "Challenging Organic Syntheses Inspired by Nature—from Natural Products Chemistry to Drug Discovery." The Faculty of Biochemistry, Biophysics and Biotechnology of Jagiellonian University is a beneficiary of structural funds from the European Union (grant no. POIG.02.01.00-12-064/08, "Molecular Biotechnology for Health") and is a partner of the Leading National Research Center supported by the Ministry of Science and Higher Education of the Republic of Poland.

The funders had no role in study design, data collection and analysis, decision to publish, or preparation of the manuscript.

REFERENCES

1. van der Hoek L, Pyrc K, Jebbink MF, Vermeulen-Oost W, Berkhout RJ, Wolthers KC, Wertheim-van Dillen PM, Kaandorp J, Spaargaren J, Berkhout B. 2004. Identification of a new human coronavirus. Nat Med 10:368–373. https://doi.org/10.1038/nm1024.
2. Konca C, Korukluoglu G, Tekin M, Almis H, Bucak İ Uygun H, Altas AB, Bayrakdar F. 2017. The first infant death associated with human Coronavirus NL63 infection. Pediatr Infect Dis J 36:231–233. https://doi.org/10.1097/INF.0000000000001390.
3. Mayer K, Nellessen C, Hahn-Ast C, Schumacher M, Pietzonka S, Eis-Hübinger AM, Drosten C, Brossart P, Wolf D. 2016. Fatal outcome of human coronavirus NL63 infection despite successful viral elimination by IFN-alpha in a patient with newly diagnosed ALL. Eur J Haematol 97:208–210. https://doi.org/10.1111/ejh.12744.
4. Cabeça TK, Bellei N. 2012. Human coronavirus NL-63 infection in a Brazilian patient suspected of H1N1 2009 influenza infection: description of a fatal case. J Clin Virol 53:82–84. https://doi.org/10.1016/j.jcv.2011.09.006.
5. Oosterhof L, Christensen CB, Sengeløv H. 2010. Fatal lower respiratory tract disease with human coronavirus NL63 in an adult haematopoietic cell transplant recipient. Bone Marrow Transplant 45:1115–1116. https://doi.org/10.1038/bmt.2009.292.
6. Fouchier RA, Hartwig NG, Bestebroer TM, Niemeyer B, de Jong JC, Simon JH, Osterhaus AD. 2004. A previously undescribed coronavirus associated with respiratory disease in humans. Proc Natl Acad Sci U S A 101:6212–6216. https://doi.org/10.1073/pnas.0400762101.
7. Pyrc K, Berkhout B, van der Hoek L. 2007. The novel human coronaviruses NL63 and HKU1. J Virol 81:3051–3057. https://doi.org/10.1128/JVI.01466-06.
8. van der Hoek L, Sure K, Ihorst G, Stang A, Pyrc K, Jebbink MF, Petersen G, Forster J, Berkhout B, Uberla K. 2005. Croup is associated with the novel coronavirus NL63. PLoS Med 2:e240. https://doi.org/10.1371/journal.pmed.0020240.
9. van der Hoek L, Pyrc K, Berkhout B. 2006. Human coronavirus NL63, a new respiratory virus. FEMS Microbiol Rev 30:760–773. https://doi.org/10.1111/j.1574-6976.2006.00032.x.
10. Pyrc K, Dijkman R, Deng L, Jebbink MF, Ross HA, Berkhout B, van der

Hoek L. 2006. Mosaic structure of human coronavirus NL63, one thousand years of evolution. J Mol Biol 364:964–973. https://doi.org/10.1016/j.jmb.2006.09.074.
11. Huynh J, Li S, Yount B, Smith A, Sturges L, Olsen JC, Nagel J, Johnson JB, Agnihothram S, Gates JE, Frieman MB, Baric RS, Donaldson EF. 2012. Evidence supporting a zoonotic origin of human coronavirus strain NL63. J Virol 86:12816–12825. https://doi.org/10.1128/JVI.00906-12.
12. Tao Y, Shi M, Chommanard C, Queen K, Zhang J, Markotter W, Kuzmin IV, Holmes EC, Tong S. 2017. Surveillance of bat coronaviruses in Kenya identifies relatives of human coronaviruses NL63 and 229E and their recombination history. J Virol 91:e01953-16. https://doi.org/10.1128/JVI.01953-16.
13. Fields BN, Knipe DM, Howley PM (ed). 2013. Fields virology, 6th ed. Lippincott Williams & Wilkins, Philadelphia, PA.
14. Hofmann H, Pyrc K, van der Hoek L, Geier M, Berkhout B, Pöhlmann S. 2005. Human coronavirus NL63 employs the severe acute respiratory syndrome coronavirus receptor for cellular entry. Proc Natl Acad Sci U S A 102:7988–7993. https://doi.org/10.1073/pnas.0409465102.
15. Li W, Moore MJ, Vasilieva N, Sui J, Wong SK, Berne MA, Somasundaran M, Sullivan JL, Luzuriaga K, Greenough TC, Choe H, Farzan M. 2003. Angiotensin-converting enzyme 2 is a functional receptor for the SARS coronavirus. Nature 426:450–454. https://doi.org/10.1038/nature02145.
16. Wickramasinghe IN, de Vries RP, Gröne A, de Haan CA, Verheije MH. 2011. Binding of avian coronavirus spike proteins to host factors reflects virus tropism and pathogenicity. J Virol 85:8903–8912. https://doi.org/10.1128/JVI.05112-11.
17. Promkuntod N, Wickramasinghe IN, de Vrieze G, Gröne A, Verheije MH. 2013. Contributions of the S2 spike ectodomain to attachment and host range of infectious bronchitis virus. Virus Res 177:127–137. https://doi.org/10.1016/j.virusres.2013.09.006.
18. Pöhlmann S, Gramberg T, Wegele A, Pyrc K, van der Hoek L, Berkhout B, Hofmann H. 2006. Interaction between the spike protein of human coronavirus NL63 and its cellular receptor ACE2. Adv Exp Med Biol 581:281–284. https://doi.org/10.1007/978-0-387-33012-9_47.
19. Milewska A, Zarebski M, Nowak P, Stozek K, Potempa J, Pyrc K. 2014. Human coronavirus NL63 utilizes heparan sulfate proteoglycans for attachment to target cells. J Virol 88:13221–13230. https://doi.org/10.1128/JVI.02078-14.
20. Mathewson AC, Bishop A, Yao Y, Kemp F, Ren J, Chen H, Xu X, Berkhout B, van der Hoek L, Jones IM. 2008. Interaction of severe acute respiratory syndrome-coronavirus and NL63 coronavirus spike proteins with angiotensin converting enzyme-2. J Gen Virol 89:2741–2745. https://doi.org/10.1099/vir.0.2008/003962-0.
21. Yoshimori T, Yamamoto A, Moriyama Y, Futai M, Tashiro Y. 1991. Bafilomycin A1, a specific inhibitor of vacuolar-type H(+)-ATPase, inhibits acidification and protein degradation in lysosomes of cultured cells. J Biol Chem 266:17707–17712.
22. Misinzo G, Delputte PL, Nauwynck HJ. 2008. Inhibition of endosome-lysosome system acidification enhances porcine circovirus 2 infection of porcine epithelial cells. J Virol 82:1128–1135. https://doi.org/10.1128/JVI.01229-07.
23. Richards AL, Jackson WT. 2012. Intracellular vesicle acidification promotes maturation of infectious poliovirus particles. PLoS Pathog 8:e1003046. https://doi.org/10.1371/journal.ppat.1003046.
24. Milewska A, Ciejka J, Kaminski K, Karewicz A, Bielska D, Zeglen S, Karolak W, Nowakowska M, Potempa J, Bosch BJ, Pyrc K, Szczubialka K. 2013. Novel polymeric inhibitors of HCoV-NL63. Antiviral Res 97:112–121. https://doi.org/10.1016/j.antiviral.2012.11.006.
25. Mu FT, Callaghan JM, Steele-Mortimer O, Stenmark H, Parton RG, Campbell PL, McCluskey J, Yeo JP, Tock EP, Toh BH. 1995. EEA1, an early endosome-associated protein. EEA1 is a conserved alpha-helical peripheral membrane protein flanked by cysteine "fingers" and contains a calmodulin-binding IQ motif. J Biol Chem 270:13503–13511.
26. Dutta D, Williamson CD, Cole NB, Donaldson JG. 2012. Pitstop 2 is a potent inhibitor of clathrin-independent endocytosis. PLoS One 7:e45799. https://doi.org/10.1371/journal.pone.0045799.
27. Joshi S, Perera S, Gilbert J, Smith CM, Mariana A, Gordon CP, Sakoff JA, McCluskey A, Robinson PJ, Braithwaite AW, Chircop M. 2010. The dynamin inhibitors MiTMAB and OcTMAB induce cytokinesis failure and inhibit cell proliferation in human cancer cells. Mol Cancer Ther 9:1995–2006. https://doi.org/10.1158/1535-7163.MCT-10-0161.
28. Shirato K, Kanou K, Kawase M, Matsuyama S. 2017. Clinical isolates of human coronavirus 229E bypass the endosome for cell entry. J Virol 91:e01387-16. https://doi.org/10.1128/JVI.01387-16.
29. Reinke LM, Spiegel M, Plegge T, Hartleib A, Nehlmeier I, Gierer S, Hoffmann M, Hofmann-Winkler H, Winkler M, Pöhlmann S. 2017. Different residues in the SARS-CoV spike protein determine cleavage and activation by the host cell protease TMPRSS2. PLoS One 12:e0179177. https://doi.org/10.1371/journal.pone.0179177.
30. Casella JF, Flanagan MD, Lin S. 1981. Cytochalasin D inhibits actin polymerization and induces depolymerization of actin filaments formed during platelet shape change. Nature 293:302–305. https://doi.org/10.1038/293302a0.
31. Holzinger A. 2009. Jasplakinolide: an actin-specific reagent that promotes actin polymerization. Methods Mol Biol 586:71–87. https://doi.org/10.1007/978-1-60761-376-3_4.
32. Hopkins CR, Miller K, Beardmore JM. 1985. Receptor-mediated endocytosis of transferrin and epidermal growth factor receptors: a comparison of constitutive and ligand-induced uptake. J Cell Sci Suppl 3:173–186. https://doi.org/10.1242/jcs.1985.Supplement_3.17.
33. Warren RA, Green FA, Enns CA. 1997. Saturation of the endocytic pathway for the transferrin receptor does not affect the endocytosis of the epidermal growth factor receptor. J Biol Chem 272:2116–2121. https://doi.org/10.1074/jbc.272.4.2116.
34. Ferguson SM, De Camilli P. 2012. Dynamin, a membrane-remodelling GTPase. Nat Rev Mol Cell Biol 13:75–88. https://doi.org/10.1038/nrm3266.
35. Park JE, Li K, Barlan A, Fehr AR, Perlman S, McCray PB, Gallagher T. 2016. Proteolytic processing of Middle East respiratory syndrome coronavirus spikes expands virus tropism. Proc Natl Acad Sci U S A 113:12262–12267. https://doi.org/10.1073/pnas.1608147113.
36. MacLean-Fletcher S, Pollard TD. 1980. Mechanism of action of cytochalasin B on actin. Cell 20:329–341. https://doi.org/10.1016/0092-8674(80)90619-4.
37. Reed L, Muench H. 1938. A simple method of estimating fifty percent endpoints. Am J Epidemiol 27:493–497. https://doi.org/10.1093/oxfordjournals.aje.a118408.
38. Harding C, Heuser J, Stahl P. 1983. Receptor-mediated endocytosis of transferrin and recycling of the transferrin receptor in rat reticulocytes. J Cell Biol 97:329–339. https://doi.org/10.1083/jcb.97.2.329.
39. Schubert W, Frank PG, Razani B, Park DS, Chow CW, Lisanti MP. 2001. Caveolae-deficient endothelial cells show defects in the uptake and transport of albumin in vivo. J Biol Chem 276:48619–48622. https://doi.org/10.1074/jbc.C100613200.
40. Berniak K, Rybak P, Bernas T, Zarębski M, Biela E, Zhao H, Darzynkiewicz Z, Dobrucki JW. 2013. Relationship between DNA damage response, initiated by camptothecin or oxidative stress, and DNA replication, analyzed by quantitative 3D image analysis. Cytometry A 83:913–924. https://doi.org/10.1002/cyto.a.22327.
41. Bolte S, Cordelières FP. 2006. A guided tour into subcellular colocalization analysis in light microscopy. J Microsc 224:213–232. https://doi.org/10.1111/j.1365-2818.2006.01706.x.